Electromagnetic transition rates in high-spin bands in ^{136}Nd

S. Mukhopadhyay,[1,2] D. Almehed,[1] U. Garg,[1] S. Frauendorf,[1] T. Li,[1] P. V. Madhusudhana Rao,[1,*] X. Wang,[1,3] S. S. Ghugre,[2] M. P. Carpenter,[3] S. Gros,[3] A. Hecht,[3,4] R. V. F. Janssens,[3] F. G. Kondev,[5] T. Lauritsen,[3] D. Seweryniak,[3] and S. Zhu[3]

[1]*Physics Department, University of Notre Dame, Notre Dame, Indiana 46556, USA*

[2]*UGC-DAE Consortium for Scientific Research, Kolkata Centre, Kolkata 700098, India*

[3]*Physics Division, Argonne National Laboratory, Argonne, Illinois 60439, USA*

[4]*Department of Chemistry and Biochemistry, University of Maryland, College Park, Maryland 20742, USA*

[5]*Nuclear Engineering Division, Argonne National Laboratory, Argonne, Illinois 60439, USA*

(Received 11 July 2008; published 17 September 2008)

Lifetimes have been measured for transitions in the two multiquasiparticle rotational bands in the nucleus ^{136}Nd. The extracted transition probabilities are compared with results of tilted-axis cranking and random-phase approximation calculations. The bands are identified as being built on two distinct quasiparticle configurations, with very different associated transition rates. These findings are contrary to an earlier suggestion that the bands form a chiral-band pair in this even-even nucleus.

DOI: 10.1103/PhysRevC.78.034311 PACS number(s): 21.10.Tg, 21.60.Ev, 23.20.Js, 27.60.+j

Rotational bands have for a long time been one of the best ways to gain an understanding of the underlying deformation and single-particle structure in open-shell nuclei and of the role of symmetries and symmetry breaking in these systems [1]. Recently, several near-degenerate $\Delta I = 1$ bands with the same parity have been found in odd-odd and even-odd nuclei in the $A \sim 105$, $A \sim 135$, and $A \sim 190$ regions, where nuclei have generally been expected to assume a triaxial shape. Some of these structures have been interpreted as chiral rotational bands on the basis of the mean field tilted-axis cranking (TAC) model [2–4], the two-particle-plus-rotor model [5,6], or extensions of the interacting boson approximation model [7,8]. Chiral rotation can appear in triaxial nuclei when protons and neutrons align along different principal axes and the collective rotation occurs along the third axis so that the total angular momentum lies outside the three principal planes. This leads to possible left-handed and right-handed orientations of the reflection-symmetric triaxial nuclear shape relative to the angular momentum. In the static case, this would lead to two degenerate sequences of states. However, rapid conversion between the two structures typically leads to an energy splitting between the two bands that can be described as chiral vibrations. In some cases, the two bands cross over in a "chiral band crossing" where they are almost degenerate over a narrow spin range.

A pair of almost degenerate bands with negative parity was reported some time ago in the even-even nucleus ^{136}Nd [9]. Two possible interpretations of these bands have been proposed: they either correspond to chiral partner bands or they are associated with different single-particle configurations. The closeness in excitation energy and the presence of strong linking transitions between the bands have been viewed as arguments favoring the chiral interpretation. On the other hand, the fact that the two bands decay out to different low-spin configurations close to the band head, and the observation that the linking transitions between the bands occur only in the "band-crossing region" argue in favor of the interpretation where different intrinsic configurations are associated with the bands.

Lifetime measurements for the transitions in these bands in ^{136}Nd have now been performed. The electromagnetic transition probabilities associated with the two bands are found to be markedly different. In addition, new calculations in the framework of the TAC model complemented by the random-phase approximation (RPA) indicate that the two bands are associated with different configurations.

The experiment was carried out at the Argonne Tandem Linac Accelerator System (ATLAS) and employed a 175-MeV ^{40}Ar beam to populate high-spin states of ^{136}Nd with the ^{100}Mo(^{40}Ar, $4n$) reaction. The target was a 1.14-mg/cm^2-thick, isotopically enriched foil backed by a 17.9-mg/cm^2 layer of Pb to slow down and finally stop the recoiling nuclei. The choice of the beam energy was dictated by the need to optimize the population of the high-spin bands in the nuclei under investigation. Five- and higher-fold coincidence events were recorded using the Gammasphere array [10] in the stand-alone mode; the array was comprised of 100 Compton-suppressed large-volume HPGe detectors at the time of this measurement. A total of about 2.5×10^9 events were accumulated and stored for further analysis.

Because the Doppler-shift attenuation method (DSAM) involves detection of γ rays at different angles during the slowing-down process in the thick target, the power of the BLUE database approach [11] proved extremely useful in efficiently sorting the data angle by angle. Several angle versus energy matrices were generated with the precondition of coincidence between two γ rays. The starting point of the double gating were the lowest (strongest and fully stopped) two transitions in the yrast band. Initially the process was carried out by adding the next γ ray in the cascade (and removing the lowest one) as one of the two gating transitions. The process was repeated until the band heads of the high-spin bands under consideration were reached. From then on, all possible combinations of carefully chosen double gates were

*Current affiliation: Department of Nuclear Physics, Andhra University, Vishakhapatnam 530 003, India.

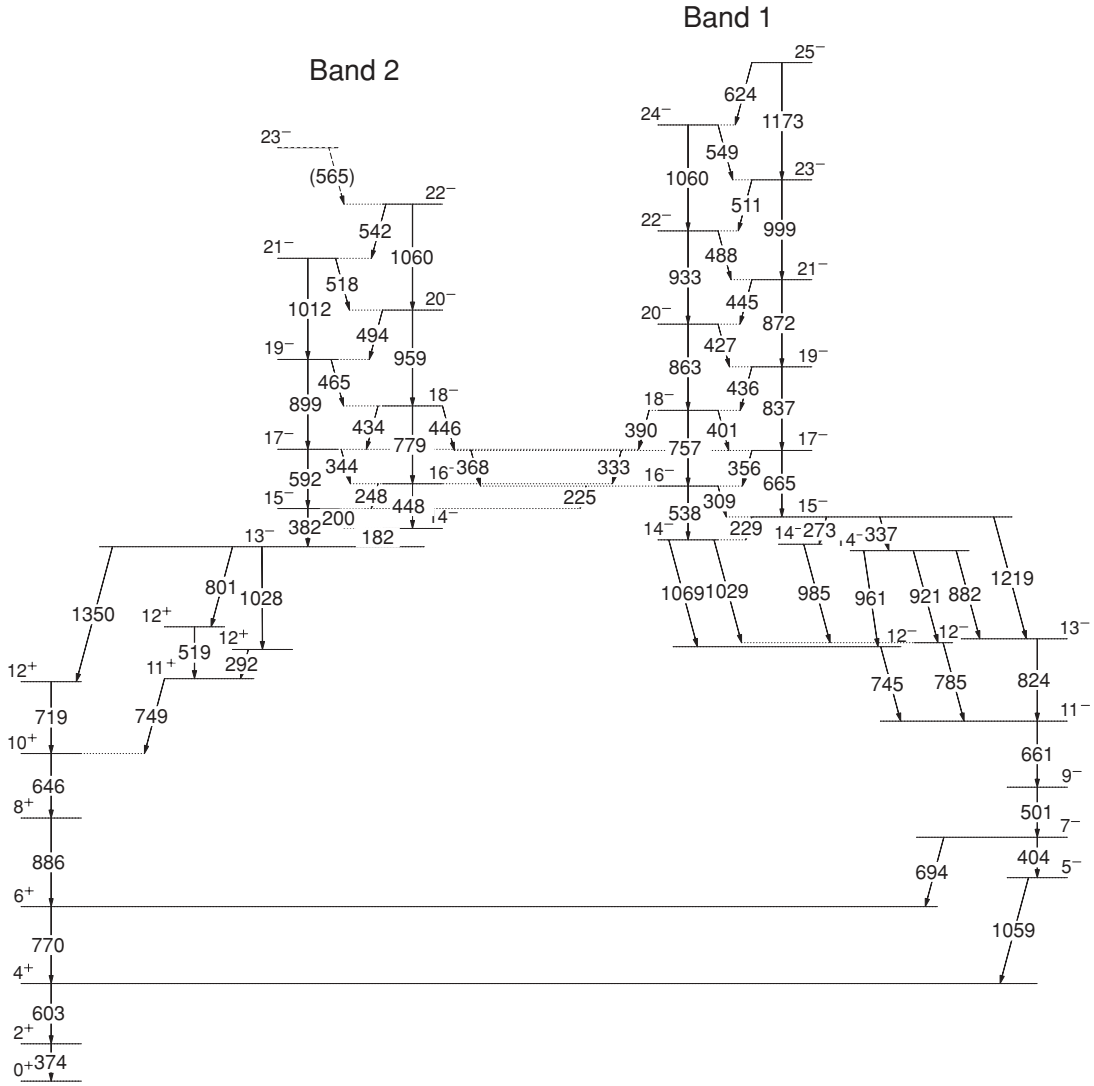

FIG. 1. Partial level scheme of ^{136}Nd showing the two high-spin bands under discussion in this article.

employed to avoid possible contamination and to extract as clean a spectrum as possible from the angle versus energy matrix for each ring (angle) of Gammasphere for further analysis of the relevant Doppler shifts. Background subtraction was performed separately for each fold, as well as for each Gammasphere ring, following the prescription of Starosta *et al*. [12].

In case of the peaks that were not fully stopped, the gate files were created by observing the peak shape distribution at each angle by projecting the previously generated double-gated angle versus energy matrix onto the energy axis. The entire peak at each angle (ring), comprising both the "stopped" and "shifted" components was then included in the gate; this eliminated a possible DSAM lifetime bias that could be introduced by omission of the tails of the peak line shape containing the fast time component of the gating transition. All gating transitions were below the level of interest.

Analysis was performed for two different angle sets, with each set containing spectra from forward, transverse, and the complementary backward angles [13]. Spectra were summed up for greater statistics for the two or three rings that were closest on the same side of the central ($\sim$90°) ring. For each angle set, lifetimes of states in both of the high-spin bands (Fig. 1) were obtained using the LINESHAPE analysis codes of Wells and Johnson [14]. A total of 5000 Monte Carlo simulations of the velocity history of the recoiling nuclei traversing the target and backing material were generated in time steps of 0.002 ps. Electronic stopping powers were calculated with the code SRIM [15], and velocity profiles were generated for each angle based on the detector geometry.

Side-feeding into each level and feeding into the top most level of each band were initially modeled as a five-transition cascade with a moment of inertia comparable to that of the in-band sequence [13,16]. The quadrupole moments of the side-feeding sequences were allowed to vary, which, when combined with the moment of inertia, acted as the effective side-feeding lifetime parameters for each level.

Starting with the top most transition in each band, the in-band and side-feeding lifetimes, the background parameters,

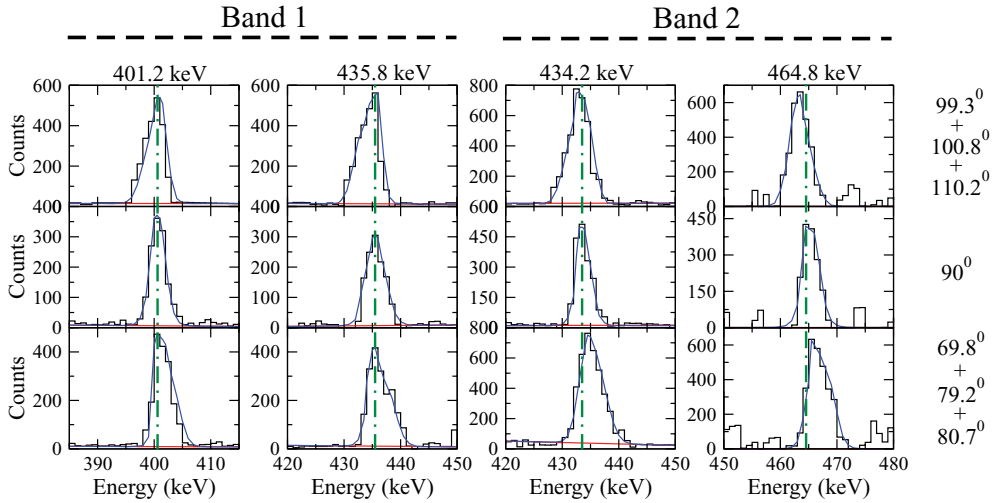

FIG. 2. (Color online) Experimental data and associated line-shape fits for the transitions in both bands under consideration. The spectra are labeled on the right-hand side with the angles of the corresponding rings.

and the contaminant-peak parameters were rendered free to vary. The forward, transverse, and backward spectra for each transition were fitted simultaneously. The best-fit background and stopped contaminant-peak parameters were then fixed, and the in-band and side-feeding lifetimes were used as an effective feeding time parameter for the next lower level in the band. Each level was added and fitted in turn, until the entire band was included in a global fit that had independently variable lifetimes for each in-band and side-feeding level [13,16]. Representative examples of DSAM fits are displayed in Fig. 2.

The branching ratios for the levels in the two high-spin bands under consideration here are presented in Table I. These have been extracted following the process discussed by Chiara *et al*. [16]. Incidentally, no information is available on these branching ratios from previous work on these bands [17,18]. The extracted lifetimes and derived transition rates are listed in Table II. Uncertainties in the lifetime measurements were derived in the usual manner from the behavior of the χ^2 fit in the vicinity of the minimum [13,16,19,20]. Systematic uncertainties associated with the modeling of the stopping powers are not included in the quoted errors and may be as large as 15%. It should be noted that to derive the absolute $B(M1)$'s, it has been assumed that the $\Delta I = 1$ transitions have pure $M1$ multipolarity. The associated transition quadrupole moments, Q_t, are comparable to those obtained for similar bands in the neighboring nuclei [8,21,22].

The formalism for the TAC calculation is described in Refs. [4,22]. Because RPA calculations have been carried out as well, a quadrupole-quadrupole (QQ) interaction Hamiltonian has been used instead of the Strutinsky renormalization (SCTAC [23]) generally employed in TAC calculations. A self-consistent TAC Hamiltonian in a harmonic oscillator basis with the QQ force acting on two major harmonic oscillator N shells ($N_{\rm low} = 4$ and $N_{\rm up} = 5$) was formulated as:

$$H' = h_0 + \sum_{m=-2}^{2} \frac{\kappa_0}{2} \sum_{N=4}^{5} \bar{Q}_m^{(N)} \bar{Q}_m^{(N)} (-)^{m+1} - \vec{\omega} \cdot \vec{J}. \quad (1)$$

TABLE I. Branching ratios for transitions in the two bands under consideration in this work. The columns represent, respectively, the excitation energies (E_x) of the depopulating levels (in keV's), the transition energies (E_γ) (also in keV's), the initial and final spins for the transitions, and branching ratios for transitions depopulating from the same level.

E_x	E_γ	$J_i^\pi - J_f^\pi$	Branching ratio
		Band 1	
5645.3	229.3	$15^- \rightarrow 14^-$	0.60(3)
	274.0	$15^- \rightarrow 14^-$	0.14(2)
	338.0	$15^- \rightarrow 14^-$	0.26(3)
5954.0	308.7	$16^- \rightarrow 15^-$	0.82(4)
	538.0	$16^- \rightarrow 14^-$	0.13(1)
	224.7	$16^- \rightarrow 15^-$	0.05(1)
6310.2	356.2	$17^- \rightarrow 16^-$	0.62(3)
	664.9	$17^- \rightarrow 15^-$	0.09(1)
	332.8	$17^- \rightarrow 16^-$	0.29(3)
6711.4	401.2	$18^- \rightarrow 17^-$	0.57(6)
	757.4	$18^- \rightarrow 16^-$	0.24(2)
	389.6	$18^- \rightarrow 17^-$	0.19(2)
7147.2	435.8	$19^- \rightarrow 18^-$	0.83(8)
	837.0	$19^- \rightarrow 17^-$	0.17(2)
		Band 2	
5729.3	199.6	$15^- \rightarrow 14^-$	0.93(5)
	382.0	$15^- \rightarrow 13^-$	0.07(1)
5977.4	248.1	$16^- \rightarrow 15^-$	0.90(3)
	447.7	$16^- \rightarrow 14^-$	0.10(1)
6321.8	344.4	$17^- \rightarrow 16^-$	0.66(4)
	592.5	$17^- \rightarrow 15^-$	0.24(2)
	367.8	$17^- \rightarrow 16^-$	0.10(1)
6756.0	434.2	$18^- \rightarrow 17^-$	0.73(7)
	778.6	$18^- \rightarrow 16^-$	0.08(1)
	445.8	$18^- \rightarrow 17^-$	0.19(2)
7221.5	465.5	$19^- \rightarrow 18^-$	0.88(9)
	899.7	$19^- \rightarrow 17^-$	0.12(2)

TABLE II. Lifetimes and electromagnetic transition probabilities for the two high-spin bands in ^{136}Nd; systematic errors associated with modeling the stopping powers are not included and may be as large as 15% (see text).

Spin I ($\hbar$)	Lifetime (ps)	$B(M1)$ (μ_n^2)	$B(E2)(e^2b^2)$	$Q_t(eb)$
		Band 1		
15^-	0.93(9)	2.7(3)	–	–
16^-	0.88(10)	1.7(2)	0.26(3)	1.73(10)
17^-	0.71(6)	1.1(1)	0.08(1)	0.95(6)
18^-	0.56(8)	0.9(2)	0.14(2)	1.26(9)
19^-	0.32(5)	1.7(3)	0.11(2)	1.11(10)
		Band 2		
15^-	1.27(6)	4.4(3)	0.54(8)	2.50(19)
16^-	0.87(8)	3.5(3)	0.51(7)	2.42(17)
17^-	0.61(7)	1.4(2)	0.44(6)	2.24(15)
18^-	0.51(7)	1.0(2)	0.04(1)	0.67(8)
19^-	0.31(5)	1.6(3)	0.05(1)	0.75(8)

h_0 is the spherical Woods-Saxon energy [2] and

$$\bar{Q}_m^{(N)} = \left(\frac{N_{\text{low}} - B}{N - B}\right)\left[\frac{2A_{n(p)}}{A}\right]^{1/3} Q_m^{(N)} \qquad (2)$$

are the dimensionless quadrupole operators for each N-shell multiplied by an N- and isospin-dependent quenching factor [4,24]. $A_{n(p)}$ are the neutron and proton numbers and $A = A_n + A_p$. The values of κ_0 (0.036 MeV) and B (0.5) that resulted in good agreement with experimental data in ^{135}Nd [22] were employed here as well. The angular velocity in the cranking term, $\vec{\omega} \cdot \vec{J}$, is defined as $\omega_1 = \omega \sin\vartheta \cos\varphi$, $\omega_2 = \omega \sin\vartheta \sin\varphi$, and $\omega_3 = \omega \cos\vartheta$, where ϑ and φ are the tilt angles [2]. The effects of pairing, which are expected to be small for these high spin, four-quasiparticle configurations, have been ignored.

The RPA calculates the harmonic excitations around the mean field minimum that in this case corresponded to $\epsilon_2 = 0.23$–0.25 and $\gamma = 25°$–$30°$, values very close to those obtained earlier for the chiral bands in ^{135}Nd [22]. The calculations will describe the system as long as one is in the chiral vibrational regime, well before the transition to static chiral rotation occurs. The Hamiltonian H is rewritten in RPA by only keeping terms up to second order in the boson operators [4,25]. The RPA equations

$$[H_{\text{RPA}}, O_\lambda^\dagger] = E_{\text{RPA}} O_\lambda^\dagger \qquad (3)$$

are solved using the strength function method of Refs. [25,26].

Figure 3 presents the energy as a function of spin for the bands of interest in ^{136}Nd. The two negative-parity bands 1 and 2 cross each other at spin I $\sim 17\hbar$. Strong linking transitions between the two bands also occur around this spin value.

TAC calculations were performed for several configurations. The best agreement with the experimental energies is achieved with configurations involving either two aligned $h_{11/2}$ protons combined with a negative-parity $h_{11/2}d_{3/2}$ neutron excitation, or two aligned $h_{11/2}$ neutrons and a negative-parity $h_{11/2}g_{7/2}$ proton excitation. The TAC results reproduce the rotational energies of the bands rather well, as can be seen in Fig. 3. The energy plot would suggest that, at low spins, band 2 has a $\pi h_{11/2}^2 \otimes \nu h_{11/2}d_{3/2}$ configuration and assumes a $\pi h_{11/2}g_{7/2} \otimes \nu h_{11/2}^2$ configuration beyond the band crossing; for band 1, the situation is reversed. If the bands are indeed built on different configurations, the location and spin of the band crossing is very sensitive to the details of the single-particle levels and to the deformation. It is, therefore, not surprising that the calculations fail to reproduce the details of the band crossing. Indeed, the fact that the calculations indicate two bands very close in energy and with similar spins can in itself be regarded as constituting good agreement between theory and experiment.

Reduced $B(M1)$ and $B(E2)$ transition probabilities were calculated from the resulting lifetimes and experimental

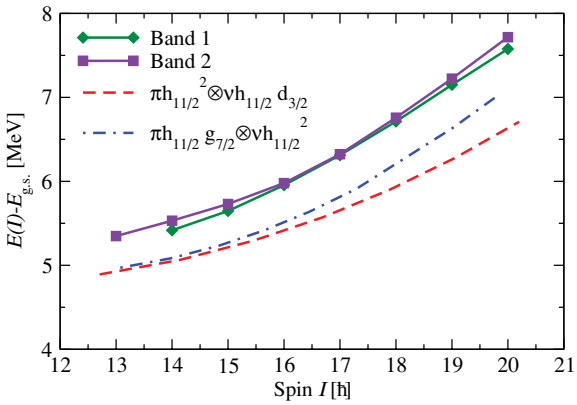

FIG. 3. (Color online) Measured and calculated energies relative to the ground state as a function of spin for the two bands in ^{136}Nd.

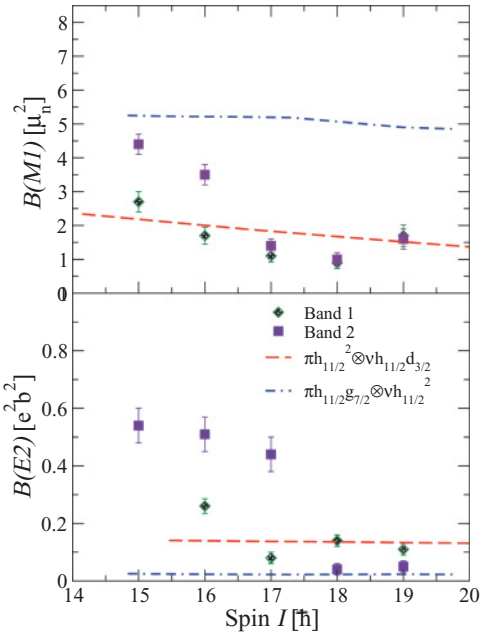

FIG. 4. (Color online) Calculated and measured $M1$ (upper panel) and $E2$ (lower panel) transition rates in the two bands. The error bars are statistical only and do not include the ∼15% error associated with the uncertainty in modeling the stopping powers (see text).

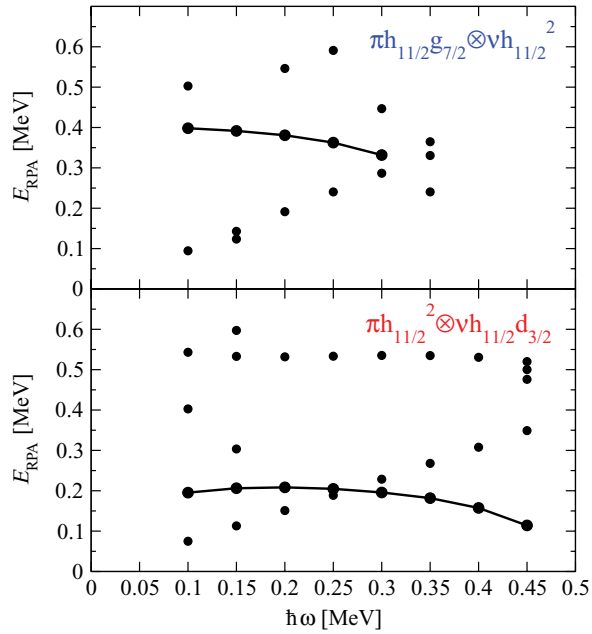

FIG. 5. (Color online) The RPA phonon energy as a function of rotational frequency for the calculated configurations. The most collective phonon states are connected by a solid line. The scattered dots represent other RPA solutions.

branching ratios. The experimental and calculated in-band transition probabilities are displayed in Fig. 4. It can be seen that the transition rates are rather different for the two bands, although the $B(M1)$ values become close when the two bands are closest in excitation energy. The $B(M1)$ values follow the ones computed for the $\pi h_{11/2}^2 \otimes \nu h_{11/2} d_{3/2}$ configuration beyond the point of closest approach ($I = 17\hbar$). The $B(E2)$ values for the two bands always differ by factors of 2 to 3 and the calculations with the two different configurations appear to come closer to the experimental data points above $I = 17\hbar$. A comprehensive interpretation of the transitions rates is complicated by the fact that the experimental data are mainly available in the band-crossing region where one cannot expect to get a good agreement with theory because band mixing is not included in the calculations.

The RPA calculations for both bands result in several low-lying RPA phonons built on each configuration. Most of these solutions are dominated by a pure particle-hole excitation and are noncollective in character. However, for each configuration, there also exists one low-lying RPA solution with rather strong collective properties. By analyzing the quadrupole transition matrix of each component, it can be shown that these solutions represent mainly a reorientation of the deformed shape relative to the angular momentum vector. This, as reported previously for the chiral bands in ^{135}Nd, can be interpreted as a chiral vibration [4,22]. The energies of these lowest collective RPA phonons are, typically, 100–400 keV, as can be seen in Fig. 5.

In the RPA calculation for the $\pi h_{11/2} g_{7/2} \otimes \nu h_{11/2}^2$ configuration, there is a fragmentation of the strength into several states at $\hbar\omega = 0.35$ MeV. The fact that there are competing low-lying collective as well as noncollective RPA solutions might indicate that these states are fragmented and/or irregular and, therefore, difficult to observe experimentally.

In summary, electromagnetic transition probabilities for transitions in two high-spin bands in ^{136}Nd have been measured. These bands were previously identified as possibly constituting a composite chiral pair. However, large differences in the measured transition probabilities are inconsistent with this interpretation. By comparing the experimental observations with TAC calculations, the two bands can be understood as corresponding to two different configurations undergoing band mixing due to the almost degenerate excitation energies. This interpretation also explains why the two bands de-excite toward different low-spin structures. However, both configurations discussed in this article have collective chiral vibrations built on top of them at excitation energies varying from 100 to 400 keV, leaving open the possibility of observing chirality in ^{136}Nd in the future.

One of the authors (S.M.) expresses his gratitude to Dr. C. J. Chiara for several very helpful discussions on the LINESHAPE codes. This work was supported in part by the US National Science Foundation (grant nos. PHY04-57120 and INT-0111536); by the Department of Science and Technology, Government of India (grant no. DST-NSF/RPO-017/98); by the U.S. Department of Energy, Office of Nuclear Physics, under contract nos. DE-AC02-06CH11357 and DE-FG02-95ER40934; and by the University of Notre Dame and the ANL-UND Nuclear Theory Initiative.

[1] S. Frauendorf, Rev. Mod. Phys. **73**, 463 (2001).
[2] V. I. Dimitrov, S. Frauendorf, and F. Dönau, Phys. Rev. Lett. **84**, 5732 (2000).
[3] P. Olbratowski, J. Dobaczewski, J. Dudek, and W. Plociennik, Phys. Rev. Lett. **93**, 052501 (2004).
[4] D. Almehed and S. Frauendorf, arXiv:0709.0969.
[5] S. Frauendorf and J. Meng, Nucl. Phys. **A617**, 131 (1997).
[6] K. Starosta *et al*., Phys. Rev. C **65**, 044328 (2002).
[7] D. V. S. Brant, D. Vretenar, and A. Ventura, Phys. Rev. C **69**, 017304 (2004).
[8] D. Tonev *et al*., Phys. Rev. Lett. **96**, 052501 (2006).
[9] E. Mergel *et al*., Eur. Phys. J. A **15**, 417 (2002).
[10] I.-Y. Lee, Nucl. Phys. **A520**, 641c (1990).
[11] M. Cromaz *et al*., Nucl. Instrum. Methods A **462**, 519 (2001).
[12] K. Starosta *et al*., Nucl. Instrum. Methods A **515**, 771 (2003).
[13] C. J. Chiara *et al*., Phys. Rev. C **61**, 034318 (2000).
[14] J. Wells and N. Johnson, Report No. ORNL-6689 p. 44 (1991) (unpublished).
[15] J. F. Ziegler, J. P. Biersack, and U. Littmark, *The Stopping and Range of Ions in Solids* (Pergamon, New York, 1985).
[16] C. J. Chiara *et al*., Phys. Rev. C **64**, 054314 (2001).
[17] A. A. Sonzogni, Nucl. Data Sheets **95**, 837 (2002).
[18] B. Singh *et al*., Nucl. Data Sheets **97**, 241 (2002).
[19] N. Johnson *et al*., Phys. Rev. C **55**, 652 (1997).
[20] U. Garg *et al*., Phys. Lett. **B180**, 319 (1986).
[21] D. T. Joss *et al*., Phys. Rev. C **58**, 3219 (1998).
[22] S. Mukhopadhyay *et al*., Phys. Rev. Lett. **99**, 172501 (2007).
[23] S. Frauendorf, Nucl. Phys. **A677**, 115 (2000).
[24] M. Baranger and K. Kumar, Nucl. Phys. **A110**, 490 (1968).
[25] P. Ring and P. Schuck, *The Nuclear Many-Body Problem* (Springer, New York, 1980).
[26] J. Kvasil and R. Nazmitdinov, Sov. J. Part. Nuclei **17**, 265 (1986).